Article:
Nkiaka, E. orcid.org/0000-0001-7362-9430 and Okafor, G.C. orcid.org/0000-0002-2417-713X (2024) Changes in climate, vegetation cover and vegetation composition affect runoff generation in the Gulf of Guinea Basin. Hydrological Processes, 38 (3). e15124. ISSN 0885-6087

https://doi.org/10.1002/hyp.15124

Received: 18 October 2023 | Revised: 1 March 2024 | Accepted: 6 March 2024

DOI: 10.1002/hyp.15124

RESEARCH ARTICLE

WILEY

Changes in climate, vegetation cover and vegetation composition affect runoff generation in the Gulf of Guinea Basin

Elias Nkiaka[1,2] | Gloria Chinwendu Okafor[3]

[1]Department of Geography, University of Lincoln, Brayford Pool Campus, Lincoln, UK

[2]Department of Geography, University of Sheffield, Sheffield, UK

[3]Department of Meteorology and Climate Change, Nigeria Maritime University, Okerenkoko, Delta State, Nigeria

Correspondence
Elias Nkiaka, Department of Geography, University of Lincoln, Brayford Pool Campus, Lincoln LN6 7TS, UK.
Email: enkiaka@lincoln.ac.uk

Funding information
Leverhulme Trust, Grant/Award Number: ECF–097–2020

Abstract

Although considerable effort has been deployed to understand the impact of climate variability and vegetation change on runoff in major basins across Africa, such studies are scarce in the Gulf of Guinea Basin (GGB). This study combines the Budyko framework and elasticity concept along with geospatial data to fill this research gap in 44 nested sub-basins in the GGB. Annual rainfall from 1982 to 2021 show significant decreasing and increasing trends in the northern and southern parts of the GGB, respectively. Annual potential evapotranspiration (PET) also shows significant increasing trends with higher magnitudes observed in the northern parts of the GGB. Changing trends in climate variables corroborates with shift to arid and wetter conditions in the north and south, respectively. From 2000 to 2020 vegetation cover estimated using enhanced vegetation index (EVI) shows significant increasing trends in all sub-basins including those experiencing a decline in annual rainfall. Vegetation composition measured using vegetation continuous fields (VCFs) from 2000 to 2020 show an increase in tree canopy cover (TC), a decline in short vegetation cover and marginal changes in bare ground cover (BG). Elasticity coefficients show that a 10% increase in annual rainfall and PET may lead to a 33% increase and 24% decline in runoff, respectively. On the other hand, a 10% increase in EVI may lead to a 4% decline in runoff while a 10% increase in TC, SV and BG may reduce runoff by 4% and increase runoff by 3% and 2%, respectively. Even though changes are marginal, decomposing vegetation into different parameters using EVI and VCFs may lead to different hydrological effects on runoff which is one of the novelties of this study that may be used for implementing nature-based solutions. The study also demonstrates that freely available geospatial data together with analytical methods are a promising approach for understanding the impact of climate variability and vegetation change on hydrology in data-scarce regions.

KEYWORDS

Budyko framework, Central Africa, data-scarce regions, elasticity concept, enhanced vegetation index, vegetation continuous fields

1 | INTRODUCTION

Runoff is an essential resource used for irrigation and food production, water supply, industry, hydropower production and for sustaining environmental flows (Baggio et al., 2021; D'Odorico et al., 2018). It is also critical for flood and drought forecasting to minimize negative socio-economic impact (Brunner et al., 2021; Emerton et al., 2018). However, climate change and variability characterized by the intensification of the global hydrological cycle and changes in rainfall patterns may alter the partitioning of precipitation into runoff and actual evapotranspiration (ET) with subsequent effects on water availability at different scales (Allan et al., 2020; Yang et al., 2021; Zheng et al., 2019). Vegetation cover change and other anthropogenic activities also exert substantial impact on the partitioning of precipitation into runoff and ET (Lu et al., 2022; Luo et al., 2020; Wang & Stephenson, 2018). As such, a better understanding of the different climatic and environmental factors influencing runoff generation may be critical for sustainable water management and adaptation planning.

Several studies have investigated the impact of climate variability and vegetation change on runoff (Luo et al., 2020; Wang & Stephenson, 2018). However, most existing studies focused on the impact of vegetation cover change (Gbohoui et al., 2021; Lu et al., 2022), whereas the impact of changes in vegetation composition (i.e., the proportion of different vegetation types) on runoff have received less attention. Vegetation composition is measured using vegetation continuous fields (VCFs) and include tree canopy cover (TC), short vegetation cover (SV) and bare ground cover (BG). In fact, several studies have shown that changes in vegetation composition may result in distinct hydrological consequences due to differences in root water uptake and rainfall interception by canopy among vegetation types (Chen et al., 2021; Iroumé et al., 2021; Neill et al., 2021; Yue et al., 2021). Therefore, in addition to understanding the impact of climate variability and vegetation cover change, there is also a need to understand how changes in vegetation composition may affect runoff. Such information may be useful for implementing nature-based solutions such as reforestation to mitigate the effects of climate change.

The most common methods for assessing the impact of climate variability and vegetation change on water resources include hydrological models (Ebodé et al., 2022; Yonaba et al., 2021), multivariable statistical methods (Gebremicael et al., 2019a; Shawul et al., 2019), experimental approaches involving paired catchment studies (Cheng et al., 2017; Ferraz et al., 2021) and analytical techniques such as the elasticity concept and Budyko framework (Gbohoui et al., 2021; Hasan et al., 2018; Wamucii et al., 2021). Despite the uncertainties associated with hydrological model outputs, they remain the most widely used method for assessing the impact of climate variability and vegetation change on water resources due to their ability to explain physical processes to some extent (Addor & Melsen, 2019). However, hydrological models require considerable input data such as observed runoff for model calibration and validation thus, limiting their application in poorly gauged basins (Herrera et al., 2022; Nkiaka et al., 2018). On the other hand, experimental methods involving paired catchment studies require longer time and resources. As such, the use of analytical methods to quantify the impact of climate variability and vegetation change on runoff is becoming increasingly popular (Gbohoui et al., 2021; Hasan et al., 2018). Unlike hydrological models, analytical methods use mathematical equations for impact assessment under the assumption that the catchment water balance remain under hydrological steady-state conditions for a long period without significant climate and vegetation changes. However, they cannot provide a detailed explanation of the underlying physical processes taking place in the catchment. Despite this limitation, their main advantage is that they do not require much input data to produce results that are practically useful in most hydrological applications (Hasan et al., 2018; Mianabadi et al., 2020). This makes the application of such methods suitable in data-scarce regions.

Although substantial efforts have been deployed to assess the impact of climate variability and vegetation change on runoff in most major hydrological basins in Africa (Bennour et al., 2023; Chawanda et al., 2023; Hasan et al., 2018), such studies are rare in the Gulf of Guinea Basin (GGB). The few studies that have attempted to fill this research gap in the region have focused on individual sub-basins (Bogning et al., 2021; Ebodé, 2023; Ebodé et al., 2022). The limited number of studies result to a dearth of knowledge on the hydrology of the GGB and the impact of climate change and variability and vegetation change on runoff, thereby impeding adaptation planning. Nevertheless, recent large-scale hydrometeorological disasters in the region triggered by increasing precipitation extremes (Bichet & Diedhiou, 2018; Dike et al., 2020) and vegetation change (Yao et al., 2019) highlight the urgent need for a regional-scale assessment of the impact of climate variability and vegetation change on runoff in the GGB. Sparsity in relevant studies in the GGB may be attributed to some of the following reasons: (1) the GGB is made up of a cluster of small to medium-size catchments with no major river or lake draining the region, as such, it is often neglected in most impact studies, (2) acute scarcity of in situ hydro-climatological data in the region while the number of existing gauges have declined over the past decades (Riggs et al., 2023), (3) data from the region is often discontinuous and contains extended gaps (Nkiaka et al., 2016) and (4) access to data from some countries in the GGB is extremely difficult due to administrative bottleneck and high cost (first author personal experience). The availability of several high-resolution and long-term geospatial datasets such as the European Centre for Medium-Range Weather Forecast (ERA5), the Global Land Evaporation Amsterdam Model (GLEAM) and Climate Hazards Group InfraRed Precipitation with Station data (CHIRPS) makes this study feasible and extremely timely.

Therefore, the objectives of this study are to: (1) analyse trends in precipitation, ET and potential evapotranspiration (PET) from 1982 to 2021 and vegetation change from 2000 to 2020, (2) assess shifts in hydroclimatic regimes in the GGB from 1982 to 2021 and lastly, (3) quantify the impact of climate variability, vegetation cover change and change in vegetation composition on runoff from 2000–2020 to correspond with timescale of MODIS products. The present study goes beyond the traditional single-catchment study and adopts a regional-scale approach which may be critical for understanding regional hydrology and generalizing the impact of climate variability and vegetation change on runoff.

2 | MATERIALS AND METHODS

2.1 | Study area

The GGB also referred to as "Central West Coast" in some studies (Blatchford et al., 2020) covers six countries including Angola, Congo-Brazzaville, Gabon, Equatorial Guinea, Cameroon and Nigeria with a population of about 267 million with Nigeria being the most populated (~225 million). It is located between longitude 6.70°–15°E and latitude 6° S–7.5°N covering a surface area of about 699 755 km^2 (Figure 1). It is an important ecoregion in Africa recognized for its unique ecological and biological diversity which has been attributed to

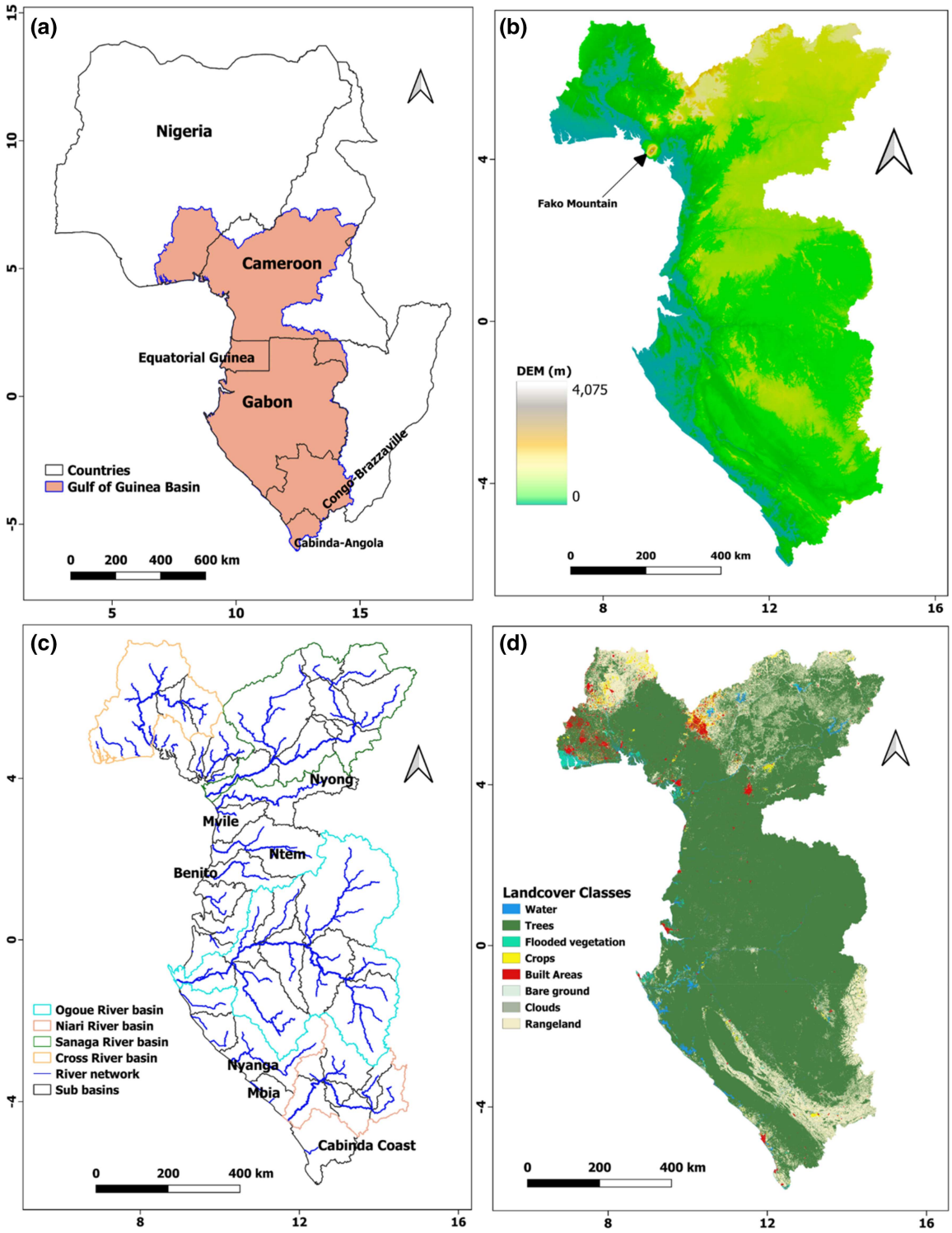

FIGURE 1 Gulf of Guinea Basin showing (a) location in Africa, (b) Digital Elevation Model, (c) sub-basins and river network and (d) Land cover in the basin. In HydroSHED, sub-basins in colour were further divided into smaller units (Figure 3c). Landcover map in Figure 3d came from Sentinel-2 10-Meter Land Use/Land Cover for the year 2022.

its varied topography providing a wide variety of habitats (Cronin et al., 2014). The highest point in the GGB is the Fako Mountain standing at 4095 m a s l and is the only active volcano in Central-West Africa. Other high peaks in the study area include Mount Muanenguba (2064 m a s l) and the Lebialem highlands. Rainfall in the GGB is mostly controlled by the West African Monsoon System (WAMS) (Dezfuli & Nicholson, 2013). Rainfall distribution is also strongly influenced by topography (Vondou et al., 2018). The GGB is one of the wettest regions in Africa with mean annual rainfall exceeding 1000 mm/year. In fact, rainfall in Debundcha located at the foothills of Fako Mountain exceeds 10 000 mm/year making it one of the wettest places on Earth (Richards et al., 1996). Mean annual temperature in the GGB is about 23.5°C. Rain-fed agriculture is the main source of livelihood for the local population. There are several agro-industrial plantations specialized in rubber, oil palm, banana and tea production. Thousands of small-scale farmers are also involved in cocoa, rubber and oil palm production. Other economic activities in the region include artisanal fishing, hunting and timber harvesting. The present study covers 44 nested sub-basins with the smallest being the Likini (1999 km^2) in Cameroon while the largest is the Ivindo (62 919 km^2) in Gabon (Figure 1c). Transboundary basins in the GGB include Cross River and Andokat (Cameroon and Nigeria), Ivindo (Gabon and Cameroon) and Ntem (Cameroon and Equatorial Guinea). Shapefiles of the different sub-basins were collected from HydroSHEDS which provides a seamless global coverage of consistently sized and hierarchically nested sub-basins using high-resolution Shuttle Radar Topographic Mission digital elevation model (Lehner & Grill, 2013). Shapefiles from HydroSHEDs have been used in several studies (Gebrechorkos et al., 2020; Odongo et al., 2019). The characteristics of the sub-basin are available in the supporting information Appendix S1.

2.2 | Data

This study adopts satellite-derived and reanalysis data for all analyses.

2.2.1 | Precipitation

Considering the complex relief in the GGB and the impact that topography has on satellite precipitation estimates (Derin et al., 2019; Gebremicael, Mohamed, Zaag, et al., 2019), three different precipitation products with different spatial resolutions were used to provide precipitation estimates. The products include CHIRPS with a spatial resolution of 0.05°, Precipitation Estimation from Remotely Sensed Information using Artificial Neural Networks (PERSIANN) with a spatial resolution of 0.25° and Global Precipitation Measurement (GPM) with a spatial resolution of 0.1°. The precipitation products were selected based on their relatively better performance in the region compared with other available products (Camberlin et al., 2019). Details of the different precipitation products can be found in their respective publications including (Funk et al., 2015) for CHIRPS, (Ashouri et al., 2015) for PERSIANN and (Skofronick-Jackson et al., 2018) for GPM. Among the three products, CHIRPS has the longest timespan from 1981, followed by PERSIANN from 1983 while GPM has the shortest timespan from 2000 to present. The ensemble mean of the three precipitation products was calculated following the time period when each product became available. Precipitation data are used for trend analysis and to calculate the aridity and evaporative ratios.

2.2.2 | Evapotranspiration

ET data was obtained from GLEAM which is a process-based semi-empirical model used for estimating surface soil moisture, root-zone soil moisture and terrestrial evaporation using satellite forcing data (Martens et al., 2017). GLEAM v3.7a was used in the present study because it covers the longest available time period (1980–2021) at an annual timescale at a spatial resolution of 0.25°. GLEAM ET estimates have been validated in many different regions in Africa (Nkiaka et al., 2022). GLEAM ET data are used to estimate the evaporative ratio.

2.2.3 | Potential evapotranspiration

PET data came from AgERA5 at a spatial resolution of 0.1° covering the period 1979 to present. AgERA5 is different from ERA5 because it is tuned to finer topography, land use pattern and land-sea delineation of the ECMWF HRES model (Boogaard et al., 2020). AgERA5 data have been validated shown to outperform ERA5 parent product in parts of Africa due to its higher spatial resolution and is therefore recommended for water resources assessment in Africa (Roffe & van der Walt, 2023). PET data from AgERA5 are used to calculate the aridity ratio.

2.2.4 | Vegetation cover

Enhanced vegetation index (EVI) is used as a proxy to measure changes in vegetation cover from 2000 to 2020. EVI used to measure vegetation greenness with higher scores indicating better vegetation quality. The advantages of EVI over the commonly used normalized difference vegetation index (NDVI) are that it (1) corrects for distortions due to aerosols, (2) minimizes canopy background variations, (3) employs a soil adjustment and (4) maintains sensitivity over dense vegetation conditions. These factors make EVI suitable in areas with dense vegetation such as the GGB. EVI data have been used to monitor vegetation change in other regions with dense vegetation (Adams & Garcia-Carreras, 2023), monitor changes in Mangrove Forests in the GGB (Lemenkova & Debeir, 2023) and to measure vegetation change across African cities (Yao et al., 2019). EVI data were obtained from Moderate Resolution Imaging Spectroradiometer (MODIS) satellite MOD13A1 V6 product at a temporal resolution of 16 days and 250 m spatial resolution from 2000 to 2020.

2.2.5 | Vegetation composition

Vegetation continuous fields (VCFs) are used to represent the proportion of vegetation composition in the GGB. It is reported that continuous variables can provide a better description of the mixture of trees, herbaceous vegetation and non-vegetated surfaces found in most pixels at all resolutions (DiMiceli et al., 2021). The present study employs VCFs from MOD44B at 250 m spatial resolution consisting of a continuous record of fractional vegetation cover including TC, SV and BG. MOD44B estimates "Percent Tree Cover" in a pixel on an annual basis and "continuous" means a continuous percent value from 0 to 100. The percent tree cover is the area proportion of tree canopy cover with tree height equal to or greater than 5 m. VCFs have been used to assess the hydrological effects of changes in vegetation components in global river basins (Chen et al., 2021). MOD44B VCFs have also been used to study the dynamics of forest cover change in east Africa (Hirvonen et al., 2022; Ryan et al., 2017). MOD44B VCFs data are used herein to understand how changes in different vegetation types affect runoff from 2000 to 2020.

2.3 | Methods

2.3.1 | River network

The river network was created in ArcGIS 10.71 using the freely available Advanced Land Observing Satellite World 3D-30 m (AW3D30) DEM produced by the Japan Aerospace Exploration Agency. AW3D30 version 3.2 with a horizontal resolution of approximately 30 m (1 arc sec) was adopted because it has been shown to outperform most freely available DEMs products in complex terrains (Moges et al., 2023).

2.3.2 | Runoff estimation

Considering the absence of in situ river discharge data in the study area and the fact that most available water resources reanalysis products have not been validated in the GGB to ascertain their performance, the long-term average runoff in each sub-basin is calculated using the water balance approach. The sub-basin water balance is therefore calculated as:

$$Q = P - \mathrm{ET}, \tag{1}$$

where Q is the runoff, P is the precipitation and ET is the evapotranspiration. The above equation is valid under the assumption that basin storage changes can be neglected over long timescales (>10 years). A similar approach has been used to estimate annual runoff in several regions (e.g., Nkiaka et al., 2022; Wamucii et al., 2021; Zhang et al., 2023).

2.3.3 | Annual runoff coefficient

Annual runoff coefficient is the ratio of annual runoff to annual precipitation estimated as:

$$\mathrm{rc} = Q/P, \tag{2}$$

where rc is the runoff coefficient, Q is runoff and P is precipitation.

2.3.4 | Data aggregation

Precipitation, PET and EVI data were aggregated to annual timescale and downloaded at their native spatial resolution using the Climate Engine (https://app.climateengine.com) (Huntington et al., 2017). Climate Engine is an open data platform used for accessing, processing, visualizing and analysing earth observation datasets via a simple web connection, thereby overcoming the computational burden of big data and providing the ability to customize data download (Huntington et al., 2017). Sub-basins shapefiles are uploaded to Climate Engine directly from a computer folder using a customized user account. ET data are downloaded from www.gleam.eu and processed using Origin Pro software. MOD44B VCFs are downloaded using Google Earth Engine platform.

2.3.5 | Trend analysis

The non-parametric Mann-Kendall test and Sen's slope estimator were respectively used for trend analysis and to quantify trend magnitude and significance at the 5% significance level. Trend analyses were conducted over a period of four decades for hydroclimatic data (1982–2021) and two decades for EVI data (2000–2020).

2.3.6 | Estimating change in vegetation composition using **VCFs**

To estimate the change in tree cover using VCFs, we calculated the mean VCFs of the first 5 years (2000–2004) and the last 5 years (2016–2020) and the difference between the two time periods is considered as the change in tree cover over the period of our assessment (2000–2020). A similar approach has been used in other studies (Chen et al., 2021; Hirvonen et al., 2022) to minimize the year-to-year variation in tree cover estimates.

2.3.7 | Budyko framework

Several studies have shown that catchment characteristics play a critical role in the partitioning of rainfall into runoff and ET (Cheng

et al., 2022; Gbohoui et al., 2021), however, understanding how they play this role remains a challenge (Cheng et al., 2022). The present study adopts the Budyko framework to understand how climate variability and catchment characteristics affect the partitioning of precipitation. The Budyko framework is based on the long-term water balance of a catchment and assumes that water and energy are the dominant factors controlling the partitioning of precipitation into runoff and ET over a long timescale. Compared with hydrological and land surface models, the Budyko framework provides a simple but robust tool to describe the partitioning of precipitation into runoff and ET (Bai et al., 2020). Due to its simplicity, robustness and limited data requirements, the Budyko framework is widely used in hydrological research (Bai et al., 2020; Gbohoui et al., 2021).

Since its original formulation (Budyko, 1974), several parametric and non-parametric Budyko-type models have been proposed in the literature. See e.g., Gan et al. (2021) for a review of different Budyko-type models. This study adopts the one parameter Fu's model because of its extensive application in Africa (Gbohoui et al., 2021; Wamucii et al., 2021) and has equally been used in several hydro-climatological studies around the world. Unlike the original non-parametric Budyko model that is applicable to longer temporal and large spatial scales (>1 year; >10 000 km^2), the parametric model is applicable to a wide range of temporal and spatial scales (Donohue et al., 2007). The Fu's model is used to partition precipitation into runoff and evapotranspiration using the evaporative ratio (ET/P) and aridity ratio (PET/P). Other secondary factors mediating this partitioning are lumped into a landscape parameter ($\omega\omega$) which includes climate variability, soil, vegetation and topographic characteristics of the basin. The Fu's equation is expressed as:

$$\frac{ET}{P} = 1 + \frac{PET}{P} - \left[1 + \left(\frac{PET}{P}\right)^{\omega}\right]^{\frac{1}{\omega}}, \tag{3}$$

where P, ET, PET and ω are precipitation, actual evapotranspiration, potential evapotranspiration and landscape parameter, respectively.

Different techniques have been used to estimate $\omega\omega$ such as machine learning (Bai et al., 2020; Cheng et al., 2022) and the least square methods (Chen et al., 2021; Gbohoui et al., 2021). The present study adopts the least square method because of its simplicity. The landscape parameter (ω) is calibrated for each sub-basin by minimizing the mean squared error between the simulated and observed evaporative ratio at annual timescale using the following objective function.

$$\text{obj} = \min \sum \left[\frac{ET}{P} - \left[1 + \frac{PET}{P} - \left[1 + \left(\frac{PET}{P}\right)^{\omega}\right]^{\frac{1}{\omega}}\right]\right]^2. \tag{4}$$

After obtaining ω values for each sub-basin, Equation (3) was re-adjusted and used to estimate new runoff values. A similar method has been used in other studies (e.g., Chen et al., 2021; Li & Quiring, 2021; Ni et al., 2022) to estimate runoff. The new runoff values are compared with runoff estimates obtained using the water balance equation. Equation (3) was therefore re-written as:

$$Q = (P^{\omega} + \text{PET}^{\omega})^{\frac{1}{\omega}} - \text{PET}. \tag{5}$$

Next the calibrated ω values were compared with values obtained from global basins by (Li et al., 2013) using the following equation:

$$\omega = 2.36M + 1.16. \tag{6}$$

In Equation (6), M represents the long-term vegetation cover conditions. Furthermore, the calibrated ω value for each sub-basin are fitted in Equation (3) to compute new ET values and the results compared with GLEAM ET estimates. A similar approach has been used to validate calibrated ω values in other studies (Cheng et al., 2022; Li et al., 2013).

Lastly, the relationship between vegetation coverage and VCFs and the calibrated ω values was evaluated using a linear regression model. The relationship between ω values and vegetation characteristics was carried out using mean ω values from 2000–2020 to correspond with the period when MODIS based products are available.

Despite the recent resurgence in the use of the Budyko framework in hydrology, it has been criticized for not been reflective of the dynamic behaviour of individual basins (Mianabadi et al., 2020) and several unanswered questions have also been raised concerning the use of Budyko framework (Berghuijs et al., 2020). Notwithstanding its weaknesses, it was adopted in this study because it has been shown to produce results that are useful in most hydrological applications even in data-scarce regions.

2.3.8 | Assessing shifts in hydroclimatic conditions in the GGB

Shifts in hydroclimatic conditions in the GGB are estimated over a period of 40 years (1982–2021) using 1982–1986 as the baseline period and 2017–2021 as the final period. A shift in hydroclimatic conditions of a basin from period 1 (t_1) to period 2* (t_2) can be represented within the Budyko space by a point moving from initial conditions [t_1: PET_1/P_1, ET_1/P_1] (Figure 2). If the movement is due to changes in aridity conditions (ΔPET/P), the movement will occur along the Budyko-type curve to a new point [t_{2^*}: PET_2/P_{2^*}, PET_2/P_{2^*}] (Figure 2). However, under a realistic condition which may be a combination of aridity change and changes in basin characteristics, the hydroclimatic conditions of the basin move to point 2 that does not fall on the initial Budyko curve. Following the movement within the Budyko space, it is possible to examine which drivers, climate aridity or basin characteristics are responsible for shifts in the hydroclimatic regime of the basin. Using the approach proposed by Jaramillo et al. (2018), such changes can be characterized by a shift (θ) and magnitude (v) calculated as follows:

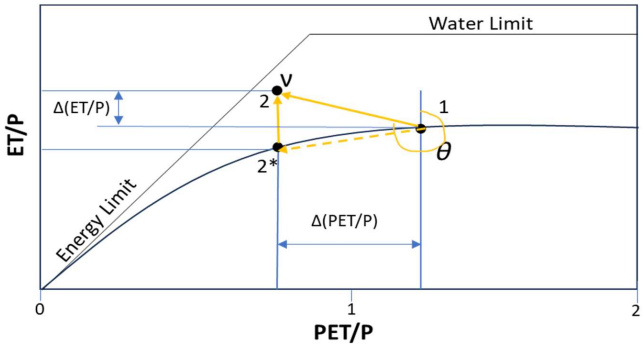

FIGURE 2 Schematic representation of the direction and magnitude change within the Budyko space. Vector (*v*) describes the hydroclimatic movement from the baseline to period 2. The length of *v* is expressed as the shift magnitude (*r*). ET, evapotranspiration; PET, potential evapotranspiration.

$$\theta = 90^{\circ} - \arctan\left[\frac{\Delta\left(\frac{ET}{P}\right)}{\Delta\left(\frac{PET}{P}\right)}\right] \Delta\left(\frac{PET}{P}\right) > 0,$$
$$\theta = 270^{\circ} - \arctan\left[\frac{\Delta\left(\frac{ET}{P}\right)}{\Delta\left(\frac{PET}{P}\right)}\right] \Delta\left(\frac{PET}{P}\right) < 0, \quad (7)$$

$$v = \sqrt{\left[\Delta\left(\frac{ET}{P}\right)\right]^2 + \left[\Delta\left(\frac{PET}{P}\right)\right]^2}. \quad (8)$$

According to Jaramillo et al. (2018) the magnitude and direction of change in the Budyko space depends on the hydroclimatic conditions of each basin and the space within which such movement occurs.

2.3.9 | Quantitative attribution of runoff change

The elasticity concept is used to quantify how a relative change in a climatic (e.g., precipitation or PET) or environmental variable (e.g., EVI) affects runoff. The method is widely used in hydrological research to measure the sensitivity of hydrological systems to changes in climatic or environmental conditions (Gbohoui et al., 2021; Hasan et al., 2018). Its extensive use in hydrology may be attributed to its clear physical meaning and simple formulation (Sankarasubramanian et al., 2001). Since the non-parametric elasticity model was introduced, several other elasticity models have been proposed. The present study adopts the least squares elasticity model because of its ability to overcome the problem associated with small sample sizes. The model is expressed as:

$$\varepsilon = \frac{\overline{X}}{\overline{Q}} \times \frac{\sum (X_i - \overline{X})(Q_i - \overline{Q})}{\sum (X_i - \overline{X})^2} = \rho_{X,Q} \times {}^{C_Q}/_{C_X}, \quad (9)$$

where Q_i is the annual runoff and X_i represent the annual climatic or environmental variable (precipitation, PET, EVI, TC, SV and BG) and $\overline{X}$ and $\overline{Q}$ represent the multiyear annual mean climatic/environmental variable and runoff values, respectively. $\rho_{X,Q}$ is the correlation coefficient between the climatic variable and runoff and C_X and C_Q are the coefficients of variation of climatic variable and surface runoff, respectively.

3 | RESULTS

3.1 | Mean annual hydroclimatology and vegetation cover

Figure 3 shows the mean annual climatology from 1982 to 2021 and mean annual vegetation cover from 2000 to 2021 over the GGB. Annual precipitation ranges from 1000 to 3000 mm/year. The highest precipitation is recorded in the north-western part of the study around Andokat sub-basin where the Fako Mountain is located while the lowest precipitation is recorded mostly in the southern parts of the GGB (Figure 3a). However, it is worth highlighting that none of the three precipitation products was able to capture annual rainfall in Debuncha, which is one of the wettest places on Earth. Runoff and runoff coefficient follow the same pattern as precipitation with runoff ranging from 61 to 1500 mm/year while annual runoff coefficients range from 0.07 to 0.55 (Figure 3b,c). PET estimates range from 1200 to 1650 mm/year with the highest PET recorded in northeastern parts of the study area around Beli, Djerem, Likini and Lom sub-basins in Cameroon (Figure 3d). PET is also substantially high in sub-basins located in the eastern part of the study area than those located in the west. ET ranges from 945 to 1400 mm/year with sub-basins located around the central part of the study area showing higher ET rates than other areas (Figure 3e). EVI scores are quasi uniform throughout the GGB with only a few sub-basins with exceptionally low EVI scores (Figure 3d). Most sub-basins in the southern part of the study area show higher EVI scores than the rest of the sub-basins except in the Andokat sub-basin.

3.2 | Trends in hydroclimatology and change in vegetation cover and composition

Figure 4 depicts trends in annual climatology and land cover change in the GGB. It can be observed that there is a strong dichotomy in precipitation trends between sub-basins located in the northern and southern parts of the GGB (Figure 4a). Most sub-basins located in Cameroon show significant decreasing trends while those located in Equatorial Guinea, Gabon, Congo-Brazzaville and northern Angola show increasing trends in annual precipitation (Figure 3a).

Trends in annual runoff and runoff coefficient follow the same pattern as precipitation trends in most sub-basins, however, there is a significant decline in runoff coefficient in sub-basins located around Cameroon (Figure 4b,c). Analyses show a strong dichotomy in annual PET trends between the eastern and the western parts of the GGB in

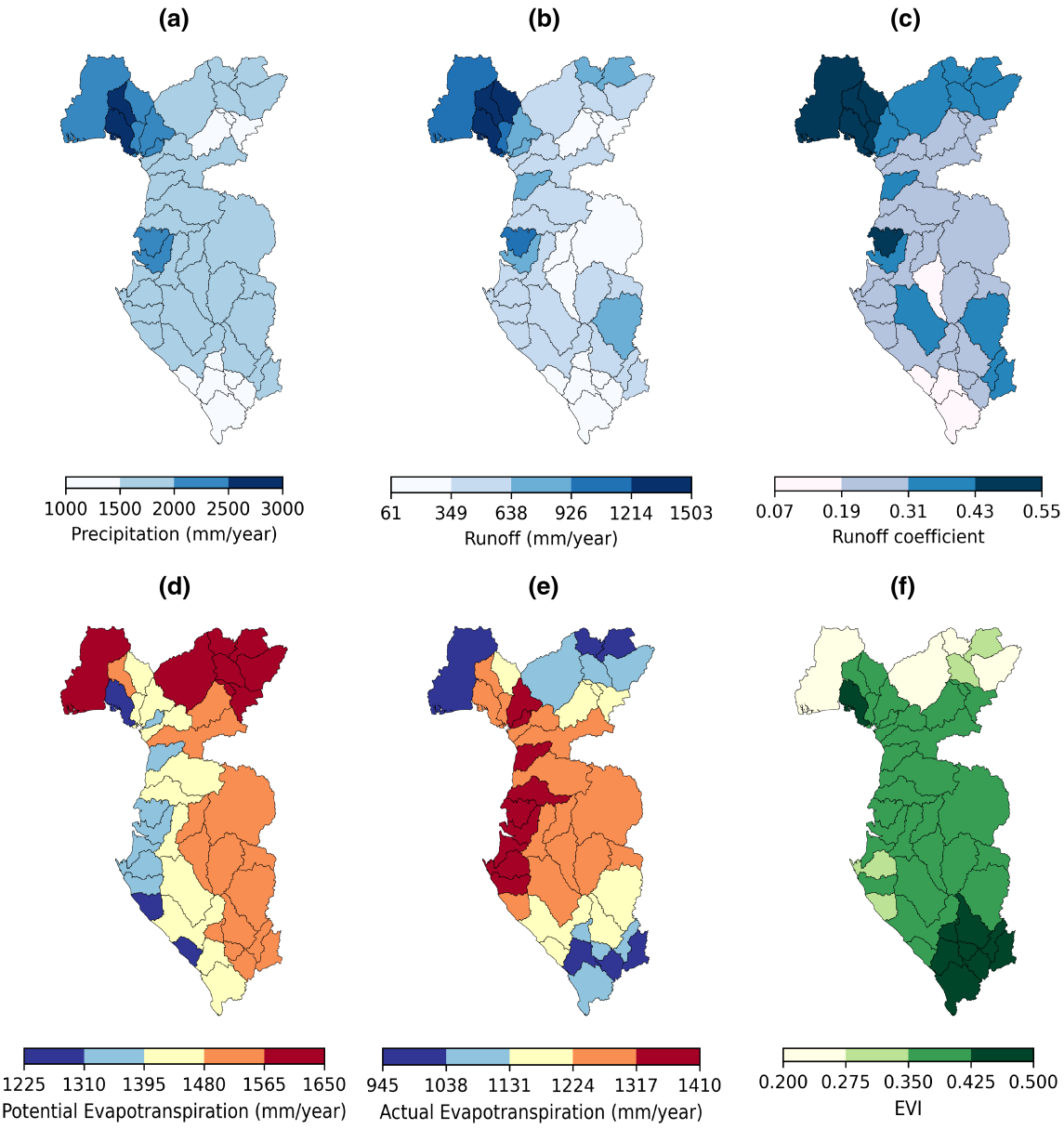

FIGURE 3 Mean annual (a) precipitation, (b) runoff, (c) runoff coefficient (d) potential evapotranspiration, (e) evapotranspiration and (f) vegetation cover. Mean climatology from 1981 to 2021 and vegetation cover from 2000 to 2020. EVI, enhanced vegetation index.

terms of trend magnitude and direction (Figure 4d). Sub-basins located in the north-east show consistent increasing trends in PET with higher magnitudes than the rest of the sub-basins (Figure 4d). Analyses also reveal strong spatial variability in ET trends throughout the study area with some sub-basins in the south and northern parts having higher trend magnitudes compared with those located around the central part of the study area (Figure 4e). Lastly, sub-basins located in the centre-eastern part of the GGB show significant increasing trends in EVI than the rest of the study area.

Figure 5 shows the long-term mean in VCFs and change in VCFs over the period 2000–2020. It can be observed that SV dominates in most of the sub-basins, followed by TC while BG appears to be the least among the different land cover types (Figure 5a–c and Appendix S1). 75% of the sub-basins exhibit an increase in TC over the study period while the rest show a decline (Figure 5d–f and Appendix S1). A corresponding percentage of sub-basins show a decrease in SV suggesting that TC gain was mostly driven by a decline in SV. Analyses also show a decline in BG in 57% of the sub-basins while the rest of the sub-basins witnessed an increase in BG over the same period. It can also be observed that sub-basins that witnessed a decline in TC also witnessed a corresponding increase in SV.

3.3 | Shifts in hydroclimatic regimes

Figure 5 shows substantial changes in the hydroclimatic conditions across all the sub-basins in the GGB from the baseline period (1982–

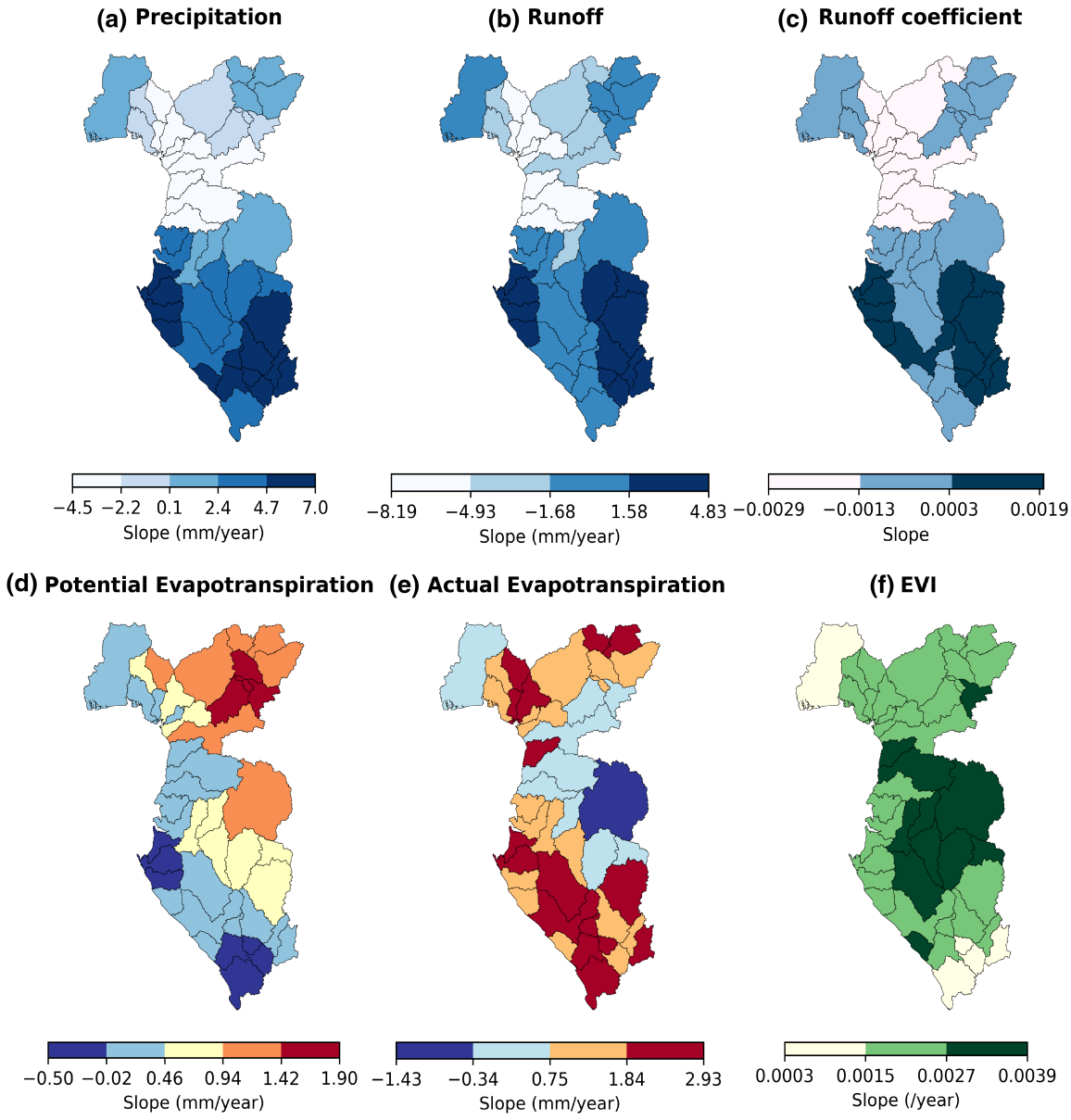

FIGURE 4 Trends in annual (a) precipitation, (b) runoff, (c) runoff coefficient (d) potential evapotranspiration, (e) actual evapotranspiration and (f) vegetation cover. Trends cover the period from 1981 to 2021 for climate variables and from 2000 to 2020 for vegetation cover. EVI, enhanced vegetation index.

1986) to the final period (2017–2021). 47% of the sub-basins moved in the rightward direction ranging from 85° to 95° with magnitude ranging from 0.02 to 0.13 indicating a shift to arid climatic conditions (Figure 6a,b). On the other hand, 53% of the sub-basins moved in the leftward direction ranging from 265° to 275° with magnitude ranging from 0.01 to 0.36 indicating a shift to a wetter climatic conditions (Figure 6b). We also observed that most of the sub-basins that shifted to arid climatic conditions are located in Cameroon while those that shifted to a wetter conditions are found in Gabon and Congo-Brazaville (Figure 6a). The shifts corresponds with the trends in annual precipitation reported in Section 3.2.

3.4 | Landscape parameter and Budyko curve

Sub-basins landscape parameter is represented by ω which also plays an important role in the partitioning of precipitation into runoff and ET. Figure 7 shows the spatial distribution of the calibrated ω values for the 44 sub-basins. It can be observed that there is high spatial variability in ω values across the GGB ranging from 4.5 to 6.75 and a mean of 5.5 with higher ω values occuring mostly in the southern part of the GGB (Figure 7a). The relationship between aridity and evaporative ratios in all the sub-basins is shown using the Budyko curve (Figure 7b). It can be observed that the GGB is located in an energy-

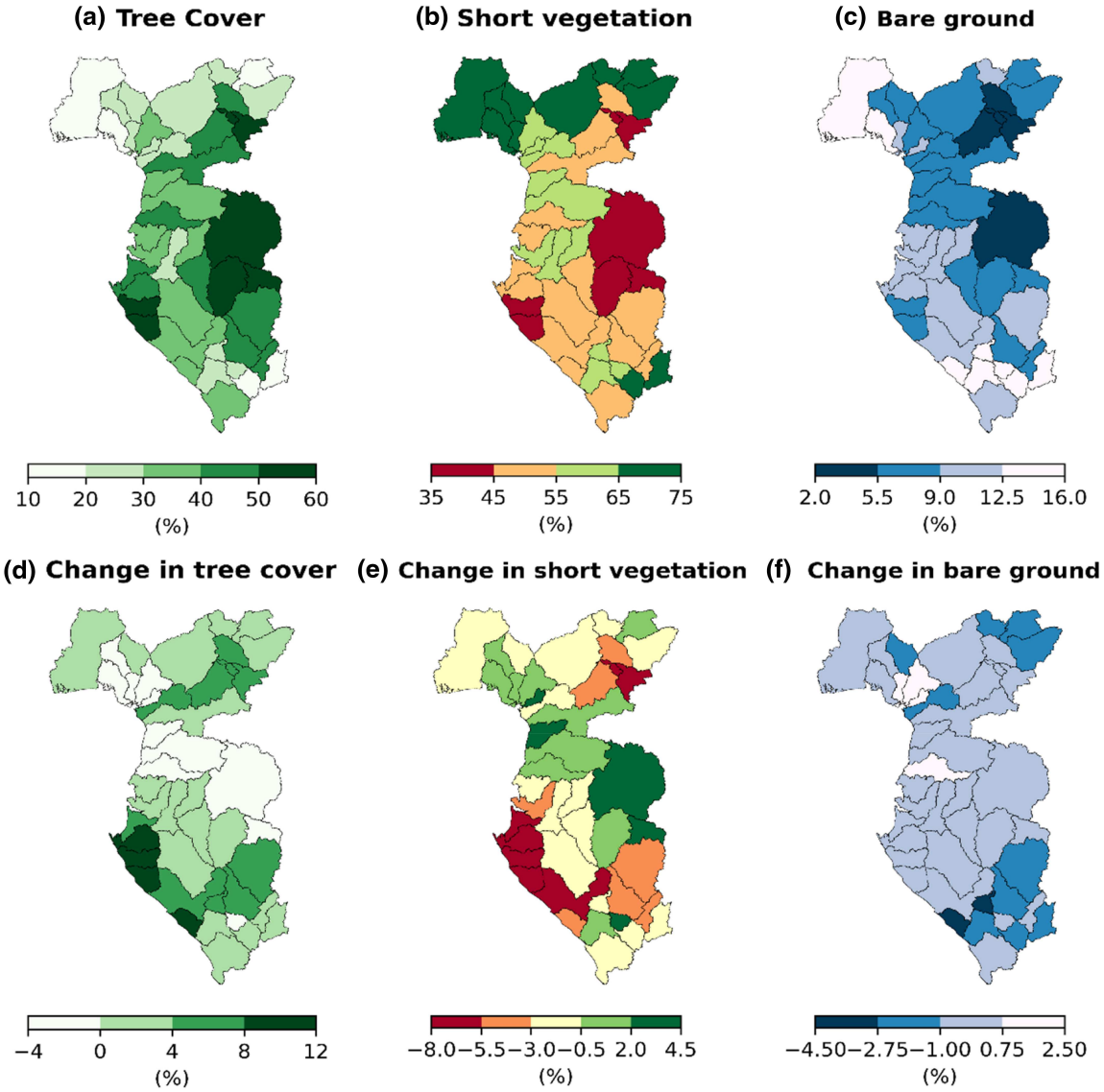

FIGURE 5 Mean annual vegetation continuous fields (VCFs) from 2000 to 2020 (a) tree cover, (b) short vegetation and (c) bare ground and change in VCFs (d) tree cover, (e) short vegetation and (f) bare ground.

limited environment as aridity ratios do not exceed 1.2 in any sub-basin (Figure 7b). This suggest that ET in the GGB may be limited by energy supply than by water availability. It can also be observed that the relationship between the aridity and evaporative ratios cannot be captured by a single Budyko curve. Although the default ω value (2.6) captures only a few sub-basins, the mean value (5.5) captures most of the sub-basins in the GGB (Figure 7b).

3.5 | Comparing calibrated landscape parameter (ω) with other models

The calibrated ω values were compared with Equation (6) derived from Li et al. (2013) for global basins. The calibrated ω values are also used to calculate new ET estimates using Equation (3) and runoff values using Equation (5). The results are then compared with GLEAM ET estimates and runoff values obtained using the basin water balance method in Equation (1). Results show a statistically significant relationship between the calibrated ω values and those derived using Equation (6) (Figure 8a). Results also show a strong and statistically significant relationship between GLEAM ET estimates and those obtained using the calibrated ω values and between water balance runoff values and runoff estimates calculated using the re-adjusted Fu model in Equation (5) (Figure 8b,c).

3.6 | Relationship between vegetation cover, VCFs and landscape characteristics

Figure 9 shows the relationship between landscape characteristics (calibrated ω values) and EVI and VCFs. It can be observed that there is a statistically significant relationship between EVI and calibrated ω values

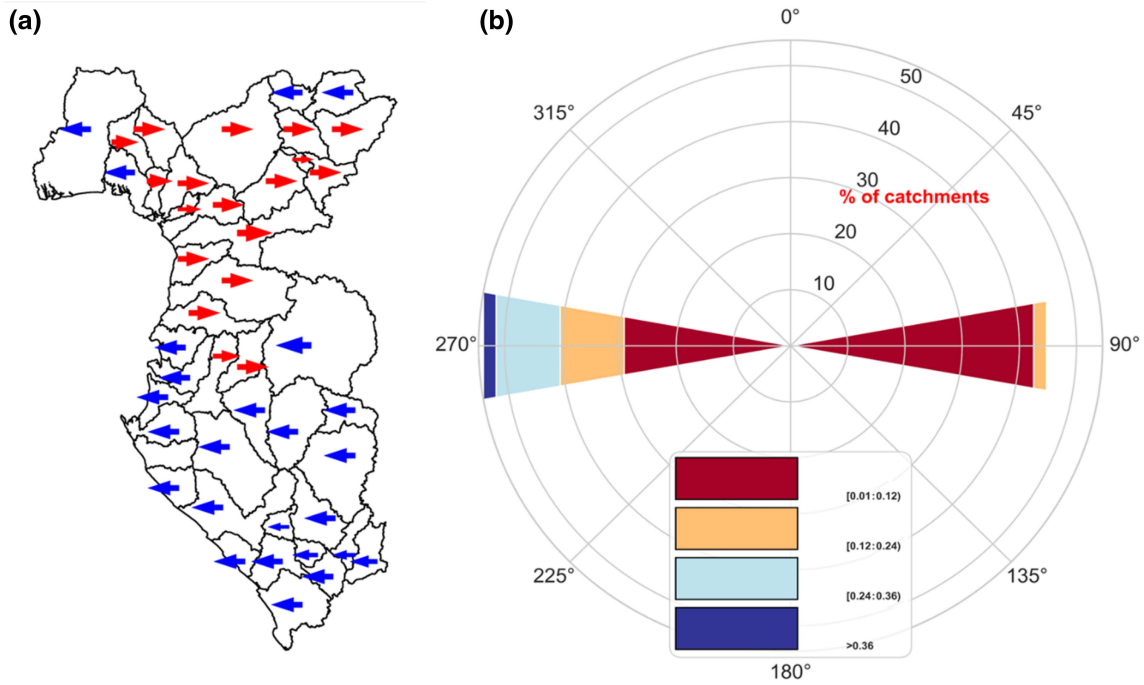

FIGURE 6 (a) Spatial distribution of sub-basin direction of shifts in the Budyko space and (b) windrose diagram showing movement within the Budyko space for all the 44 sub-basins in the Gulf of Guinea Basin resulting to changes in the aridity index (potential evapotranspiration/P) and evaporative index (evapotranspiration/P) over the baseline period 1982–1986 and 2017–2021. In (a) the red colour represent shift to more arid conditions while blue colour represent shift to wetter conditions. In (b) the range of direction is divided into 45 interval paddles that group all sub-basins moving in each direction interval. The directions start from the upper vertical and clockwise. Colour intensity describes the magnitude of the movement. Interval intensity represents the percentage of basins with a given direction and magnitude range.

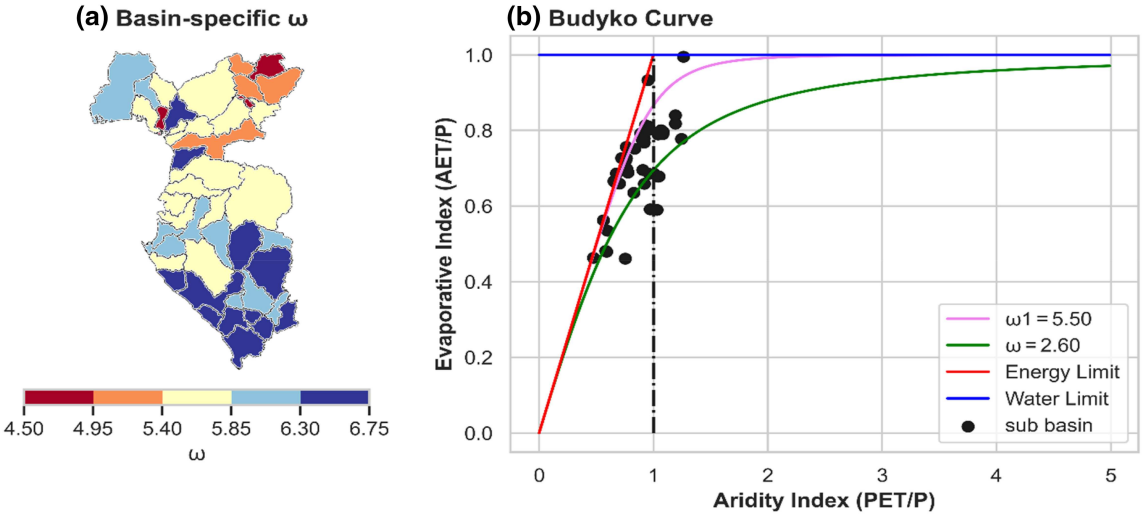

FIGURE 7 Spatial distribution of (a) calibrated ω values and (b) Budyko curve with mean calibrated ω values and default Fu parameter ω value. PET, potential evapotranspiration. AET, actual evapotranspiration.

($R^2 = 0.44$, $p < 0.05$) and a similar relationship exist between BG and calibrated ω values ($R^2 = 0.49$, $p < 0.05$) (Figure 9a,d). However, the relationship between BG and the calibrated ω values is slightly stronger than that between EVI and calibrated ω values. Analyses further reveal negative and statistically non-significant relationships between TC and SV and calibrated ω values (Figure 9b,c).

3.7 | Attribution of runoff change

Figure 10 shows the boxplots of elasticity coefficients of climate variability (precipitation and PET) and vegetation (EVI and VCFs) on runoff. It can be observed that while precipitation produce positive elasticity coefficients PET produce mostly negative elasticity

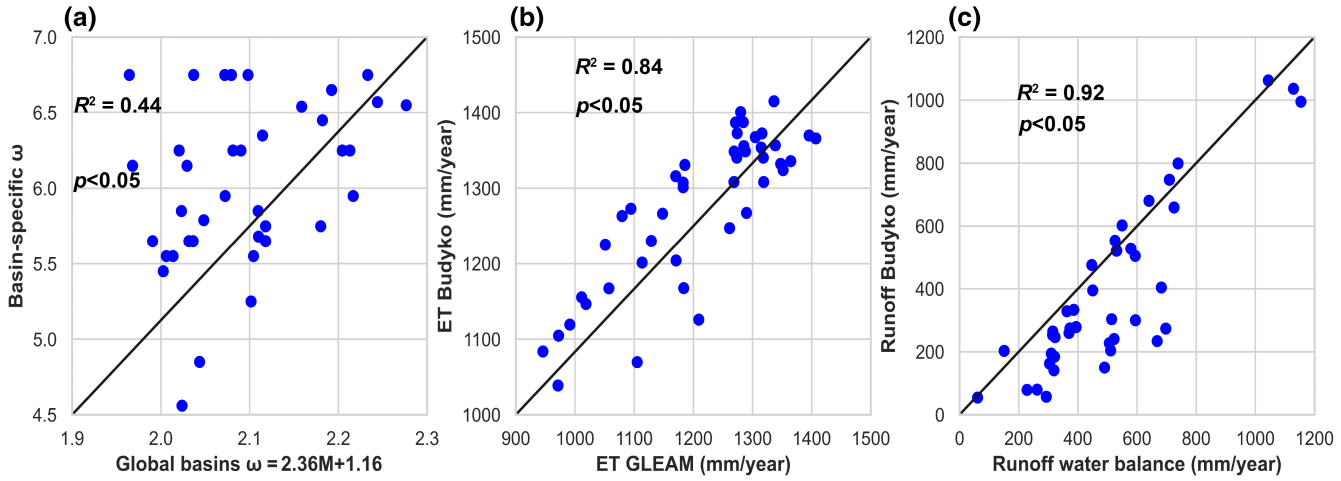

FIGURE 8 Comparison between: (a) basin-specific ω values and values derived from global basins with parameter (M) obtained from enhanced vegetation index (EVI), (b) evapotranspiration (ET) obtained using Fu equation (Equation 3) and ET data from obtained from Global Land Evaporation Amsterdam Model (GLEAM) and runoff calculated using the water balance method and runoff derived using the Fu Budyko equation.

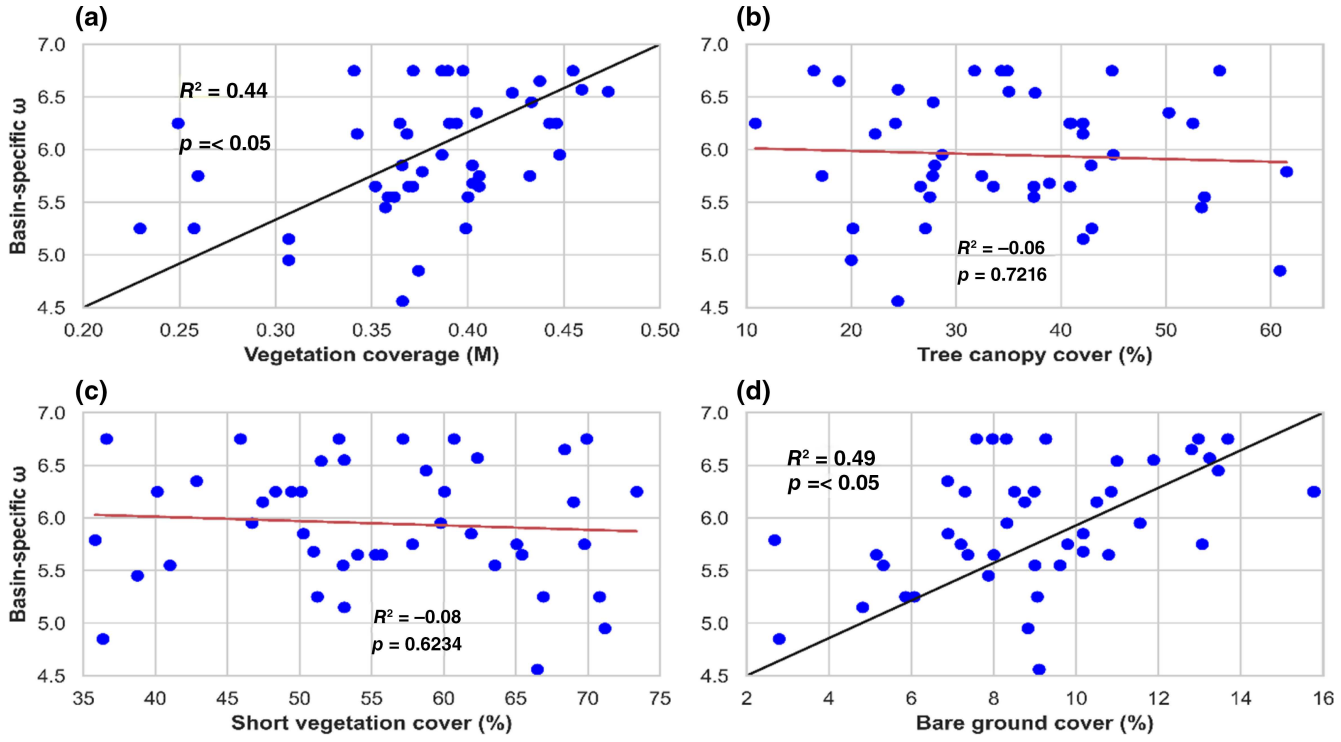

FIGURE 9 Relationship between landscape characteristics and (a) vegetation cover, (b) tree canopy cover, (c) short vegetation cover and (d) bare ground cover.

coefficients on runoff (Figure 10a). Elasticity coefficients range from 0.42 to 9.898, −20.98 to 17.61 with corresponding means of 3.26, −2.37 for precipitation and PET, respectively. For vegetation parameters, EVI and TC show negative elasticity coefficients while SV and BG show positive elasticity coefficients (Figure 10b). Elasticity coefficients for vegetation parameters range from −3.43 to 2.21, −1.74 to 0.58, −1.84 to 4.04 and − 0.71 to 2.67 with corresponding means of −0.42, −0.37, 0.34 and 0.21 for EVI, TC, SV and BG, respectively. PET has the widest spread among the climate variables while SV has the widest spread among vegetation elements (Figure 10a,b). The elasticity coefficients indicate that a 10% increase in precipitation, SV and BG will lead to 33%, 3.4% and 2% increase in runoff, respectively, whereas 10% increase in PET, EVI and TC will lead to 24%, 4.2% and 3.7% decline in runoff, respectively. Results suggest that the influence of climate variability on runoff is stronger than that of vegetation parameters.

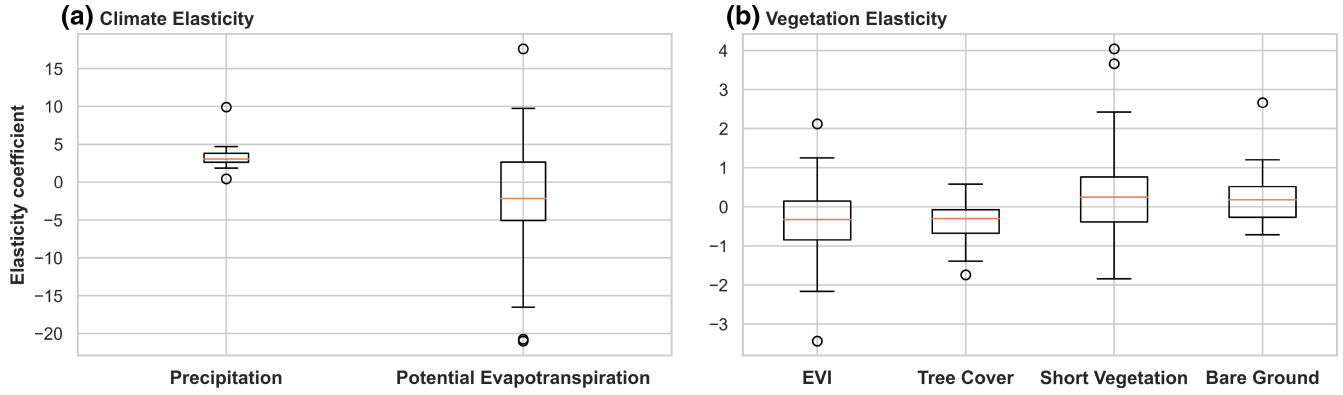

FIGURE 10 Elasticity coefficients of (a) climate variables (precipitation and potential evapotranspiration [PET]) and vegetation elements (enhanced vegetation index [EVI] and vegetation compositions [VCFs]). The elasticity coefficient relates to how much a change in precipitation, PET, EVI, tree canopy cover, short vegetation cover and bare ground cover would affect runoff generation.

4 | DISCUSSION

4.1 | Hydroclimatology

Spatial distribution of rainfall in the GGB is controlled by different factors including the WAMS (Dezfuli & Nicholson, 2013) and topographic effects (Vondou et al., 2018). Using a the arithmetic mean of three different precipitation products, our analyses show, respectively, increasing and decreasing trends in annual precipitation in the southern and northern parts of the GGB. Annual precipitation decline in the northern part of the GGB is consistent with results from other studies in the region using precipitation estimates from CHIRPS (Bichet & Diedhiou, 2018; Nkiaka, 2022) and Climate Research Unit (Ebodé, 2022). Rainfall decline in Central Equatorial Africa has been attributed partly to sea surface temperature variations over the Indo-Pacific linked with the enhanced and westward extended tropical Walker circulation (Hua et al., 2016). Increasing annual precipitation in the southern parts of the GGB (Gabon, Equatorial Guinea, Congo-Brazaville and Cabinda-Angola) is also consistent with results from another study using precipitation estimates from TAMSAT (Alahacoon et al., 2021). Increasing annual precipitation in this part of the GGB may partly be attributed to a bimodal rainfall regime in the region (Alahacoon et al., 2021). Changes in runoff and runoff coefficient may be linked to changes in precipitation patterns given that precipitation is the main factor that influences runoff in the region (Sidibe et al., 2019). Increasing trends in PET in the region have also been reported in other studies using data from CRU and were attributed to rising global surface temperatures (Abiye et al., 2019). Increasing trends in ET over the GGB are also consistent with results from a study using MODIS-derived ET estimates (Ndehedehe et al., 2018).

Shifts in hydroclimatic regimes in the GGB follow a similar pattern in annual precipitation and PET over the region. Analyses show a shift to more arid conditions in the northern part of the study area which corresponds to a decline in annual precipitation and significant increase in annual PET and a shift to wetter conditions in the southern part of the study area which also corresponds to an increase in annual rainfall and marginal (non-significant) increase in annual PET in this part of the GGB. Changes in hydroclimatic regimes in the northern and southern parts of the study area may have important implication for water management and agriculture in the GGB.

4.2 | Change in vegetation cover and composition

Increasing trends in EVI over GGB are also consistent with results from other studies investigating trends in forest growth in the region (Adams & Garcia-Carreras, 2023) and hydrological controls on vegetation dynamics over Africa (Ndehedehe et al., 2019). Both studies used EVI from MODIS and NDVI from Global Inventory Modelling and Mapping Studies. Results show significant increase in EVI across the GGB including in areas where precipitation is declining. This suggests that precipitation may not be the main factor influencing vegetation cover change in the GGB. Therefore, additional research may be needed to uncover other factors driving increasing vegetation greenness in the GGB.

Analyses show substantial changes in vegetation composition across the GGB over the period 2000–2020 with TC increasing in 75% of the sub-basins while SV declines by a corresponding percentage. The results are in-line with those obtained in other parts of the GGB using Sentinel-2 imagery and LiDAR which showed a decline in savanna vegetation by about 50% and an increase in forest cover by the same percentage from 1975 to 2020 in the Mpem & Djim National Park in Cameroon (Sagang et al., 2022). The results are also consistent with those of Wei et al. (2023) who used a combination of Advanced Very High Resolution Radiometer VCFs, MODIS VCFs, Global Forest Change product and GLOB-MAP Leaf Area Index to show increasing forest cover across Africa with Angola, Cameroon and Gabon featuring among the top hotspots of forest gain over the period 2000–2020. Increasing forest cover in the GGB may be attributed to the creation of several protected areas in the region given its rich biodiversity (Cronin et al., 2014) and considering that protected areas have been shown to increase forest cover (Ota et al., 2020). The

highest increase in tree cover is recorded in Ndogo sub-basin (Gabon) which led to a corresponding decrease in SV in the same sub-basin (Appendix S1). Sub-basins with substantial decline in TC and increasing SV include Bibamba, Nkam, Mungo and Mvile (all in Cameroon). This may be attributed to increasing plantation agriculture, which have both been identified to be a major driver of deforestation around the coastal areas of Cameroon (Ewane, 2021; Mahmoud et al., 2020). The continuous expansion of commercial agriculture around the GGB has been attributed to high returns in agricultural conversion (Carrasco et al., 2017).

4.3 | Budyko framework

Our analyses show a strong spatial variability in calibrated ω values, which reflects the varied characteristics of the landscape and climate variability in the GGB. However, the mean ω parameter (5.5) does not capture all the sub-basins while the default Fu parameter (2.6) captures only a few sub-basins. This suggest that a single ω parameter may not be used to capture the characteristics of all sub-basin which is consistent with results from other studies (Cheng et al., 2022). High ω values greater than 3 obtained in this study are consistent with results obtained in the Amazon basin (Li et al., 2013) and other tropical watersheds (Cheng et al., 2022). Analyses further reveal that the mean ω parameter obtained in the GGB is two-fold higher than the original Fu parameter. Differences between ω values obtained in this study and the default value (2.6) may be attributed to differences in basin sizes given that basin characteristics play a dominant role in the partitioning of precipitation in smaller basins while climate play a greater role in larger basins (Kingston et al., 2020). The high ω values suggest that even though the GGB is located in an energy limited environment, ET rates here are substantially high which may be attributed to high water availability, abundant forest cover and vast agricultural plantations. Extensive forest cover and agricultural plantations have been shown to strongly influence ET rates in parts of Africa (Odongo et al., 2019). The mean aridity and evaporative indexes obtained in the GGB are also within the range obtained in the neighbouring Congo basin (Li et al., 2013).

4.4 | Validation of calibrated ω values and relationship between EVI and VCFs

The calibrated ω values were compared with those obtained using Equation (6) for global basins while new ET estimates calculated using the ω values were compared with GLEAM ET data. Results show statistically significant relationship between the calibrated ω values and values obtained using Equation (6) with M representing the EVI score for each sub-basin. The significant relationship between the calibrated ω values and EVI suggest that vegetation cover may exert a strong effect on landscape characteristics in the GGB. Furthermore, the statistically significant relationship between GLEAM ET and ET values obtained using calibrated ω values suggest that the calibrated ω values are able to capture ET processes in the different sub-basins to an extent. This may be attributed to the fact that ET estimates calculated using the calibrated ω values are based on the Budyko framework that uses the energy and water limit approach and GLEAM ET estimates are also calculated using an energy-balance approach. This finding is in-line with results from an another study showing a strong relationship between Budyko-simulated ET estimates and those obtained using the energy-balance approach (Zhang et al., 2023). Results also show strong and statistically significant relationship between water balance runoff estimates and those obtained using Equation (5) which is consistent with results from other studies (e.g., Chen et al., 2021). Taking together, our analyses suggest that the calibrated ω values in this study are able to represent the major hydrological processes (ET and runoff) in the GGB to some extent.

There is also a moderate relationship between the calibrated ω values and EVI, which is consistent with results from other studies using NDVI for example, (Gbohoui et al., 2021). Similarly, there is a moderate relationship between the calibrated ω values and BG. However, the relationship between the calibrated ω values and BG is slightly stronger than that with vegetation cover. This suggest that BG represents the landscape characteristics slightly better than EVI. On the other hand, there is no relationship between ω values and TC and SV. Analyses suggest that vegetation parameters alone may not be used to represent the landscape characteristics in the GGB. This is consistent with results from other studies suggesting that factors controlling landscape parameters (ω) are complex and diverse in small basins (Bai et al., 2020).

4.5 | Attribution of runoff changes

The elasticity concept is used to quantify the impact of precipitation, PET, vegetation cover (EVI) and vegetation composition (VCFs) on runoff in the GGB. Results suggest that runoff is more sensitive to climate variability (precipitation and PET) than vegetation parameters (EVI and VCFs). This is consistent with results from other studies showing that precipitation and PET have, respectively, positive and negative elasticity coefficients on runoff (Gbohoui et al., 2021; Wang & Stephenson, 2018). Elasticity coefficients of VCFs obtained in this study are the same order of magnitude with those obtained in a global study (Chen et al., 2021). Even though the percentage change in runoff caused by changes in VCFs may be small, we found that decomposing vegetation into different parameters using EVI and VCFs produce different effects on runoff. For example, EVI and TC produce negative elasticity coefficients with almost the same magnitude. Among the VCFs, BG has highest positive elasticity coefficient on runoff while TC produce the lowest elasticity coefficient. Analyses are consistent with those from a global study indicating that TC and BG, respectively, produce negative and positive elasticity coefficients on runoff (Chen et al., 2021). The negative elasticity coefficients produced by EVI and TC are consistent with results from several studies and may be attributed to increased evapotranspiration from increasing vegetation leading to a decline in runoff (Luo et al., 2020). Meanwhile,

positive elasticity coefficients for SV and BG may be attributed land use change such as increasing plantation agriculture and urbanization, which both reduce soil infiltration capacity leading to higher runoff volumes (Bruijnzeel, 2004). The present study has demonstrated that vegetation cover and vegetation cover types influence runoff in different ways, which is one of novelties of this study and extends existing knowledge on the relationship between ecological and hydrological processes. Such information may be useful for implementing nature-based solutions such as reforestation and ecological protection. Future research may seek to understand how the different vegetation parameters influence other hydrological processes such as soil moisture and groundwater recharge.

4.6 | Uncertainties and limitations

This study uses the Budyko framework to understand the effect of climate variability and vegetation parameters on runoff in the GGB. Although the study provides a general picture of the hydroclimatic conditions and dominant hydrological processes in the GGB, we acknowledge that our results are not void of uncertainties. For example, the Budyko model has been extensively criticized as reported in the last paragraph of sub-Section 2.3.7 of this article. Furthermore, the are several sources of uncertainties inherent in the remote sensing and reanalysis datasets used in the study. Due to a lack of in situ data and considering the complex relief in the GGB, three different precipitation datasets are used to mitigate the uncertainties in precipitation products used in the study. To mitigate the biases related to the year to year variation in tree cover (Hirvonen et al., 2022), the mean VCFs of the first 5 years and the last 5 years was calculated and the difference between the two time periods was considered as the change in tree cover over the period of our assessment. EVI was adopted over the widely used NDVI to estimate vegetation cover because EVI scores are suitable in areas with dense vegetation such as the GGB.

Other sources of uncertainties in the study are from GLEAM ET data that have been reported to slightly underestimate ET in parts of Africa (Nkiaka et al., 2022). In addition, the AgERA5 data used in this study equally have its inherent biases, however it is recommended for use in water resources assessments in Africa due to its high spatial resolution (Roffe & van der Walt, 2023). Lastly, the effect of dams and reservoirs was not considered in this study and such man-made structures have been shown to alter regional climate and hydrological cycle (Cao et al., 2020). Dams and reservoirs may influence runoff elasticity and alter landscape characteristics in sub-basins where they are situated and these factors were not considered in this study. Considering the issues highlighted, results from this study should be interpreted with caution. It is our opinion that the continuous advancement in satellite technology will reduce the level of uncertainty in satellite-derived data to an extent. Nevertheless, the availability of in situ data and access to this data without administrative bottleneck and high cost will be critical in mitigating data uncertainties to adequately address recurrent hydrometeorological risks in the GGB and in other regions facing the same challenges in data availability and access.

5 | CONCLUSIONS

The objective of this study was to quantify the impact of climate variability, vegetation cover change and changes in vegetation composition on runoff in the GGB. Our analyses reveal significant changes in annual precipitation, ET and PET in the GGB. Changes in precipitation and PET trends corroborate with the Budyko model, which shows shifts towards more arid and wetter conditions, respectively, in the northern and southern parts of the GGB. Analyses also show significant increasing trends in EVI in all sub-basins, an increase in TC and a decline in SV in several sub-basins. There is a strong spatial variability in calibrated landscape parameters (ω) with analyses showing that a single Budyko type curve cannot capture all the sub-basins within the Budyko space. ET estimates calculated using the calibrated ω values show statistically significant relationship with GLEAM ET estimates. Runoff values calculated using the calibrated ω values also show strong and statistically significant relationship with water balance runoff estimates. EVI and BG both show only moderate relationship with the calibrated ω values suggesting that vegetation alone cannot account for all the landscape characteristics in the GGB. Quantifying changes in runoff using the elasticity concept show that climate variables exert a greater impact on runoff than vegetation. Precipitation exerts greater positive impact than SV and BG while PET exerts a greater negative impact than EVI and TC. The elasticity coefficients suggest that a 10% increase in precipitation, SV and BG will lead to 33%, 3.4% and 2% increase in runoff, respectively, whereas 10% increase in PET, EVI and TC will lead to 24%, 4.2% and 3.7% decline in runoff, respectively. Decomposing vegetation into different parameters using EVI and VCFs show distinct hydrological effects on runoff with EVI and TC having negative elasticity coefficients while SV and BG both have positive elasticity coefficients. Analyses show that decomposing vegetation into different parameters using EVI and VCFs may lead to different hydrological effects on runoff, which is one of the novelties of this study that may used for implementing nature-based solutions. The study also demonstrates that freely available geospatial data along with analytical methods are a promising approach for understanding the impact of climate variability and vegetation change on hydrology in data-scarce regions.

AUTHOR CONTRIBUTIONS

Elias Nkiaka: Conceptualization; Data Curation; methodology; investigation, resources, writing–review and editing; funding acquisition. **Gloria Chinwendu Okafor:** Methodology; investigation, writing–review and editing.

FUNDING INFORMATION

The first author was funded by the Leverhulme Trust Early Career Fellowship-Award Number ECF–097–2020.

CONFLICT OF INTEREST STATEMENT

The authors declare that they have no conflict of interest.

DATA AVAILABILITY STATEMENT

The data that support the findings of this study are available from Climate Engine Research App. Restrictions apply to the availability of these data, which were used under license for this study. Data are available from https://www.climateengine.org/ with the permission of Climate Engine Research App.

ORCID

Gloria Chinwendu Okafor https://orcid.org/0000-0002-2417-713X

REFERENCES

Abiye, O. E., Matthew, O. J., Sunmonu, L. A., & Babatunde, O. A. (2019). Potential evapotranspiration trends in West Africa from 1906 to 2015. *SN Applied Sciences*, *1*, 1–14.

Adams, C. E., & Garcia-Carreras, L. (2023). Detection of land-use change and rapid recovery of vegetation after deforestation in The Congo Basin. *Earth Interactions*, *27*, 220020.

Addor, N., & Melsen, L. (2019). Legacy, rather than adequacy, drives the selection of hydrological models. *Water Resources Research*, *55*, 378–390.

Alahacoon, N., Edirisinghe, M., Simwanda, M., Perera, E., Nyirenda, V. R., & Ranagalage, M. (2021). Rainfall variability and trends over the African continent using TAMSAT data (1983–2020): Towards climate change resilience and adaptation. *Remote Sensing*, *14*, 96.

Allan, R. P., Barlow, M., Byrne, M. P., Cherchi, A., Douville, H., Fowler, H. J., Gan, T. Y., Pendergrass, A. G., Rosenfeld, D., Swann, A. L. S., Wilcox, L. J., & Zolina, O. (2020). Advances in understanding large-scale responses of the water cycle to climate change. *Annals of the New York Academy of Sciences*, *1472*, 49–75.

Ashouri, H., Hsu, K.-L., Sorooshian, S., Braithwaite, D. K., Knapp, K. R., Cecil, L. D., Nelson, B. R., & Prat, O. P. (2015). PERSIANN-CDR: Daily precipitation climate data record from multisatellite observations for hydrological and climate studies. *Bulletin of the American Meteorological Society*, *96*, 69–83.

Baggio, G., Qadir, M., & Smakhtin, V. (2021). Freshwater availability status across countries for human and ecosystem needs. *Science of the Total Environment*, *792*, 148230.

Bai, P., Liu, X., Zhang, D., & Liu, C. (2020). Estimation of the Budyko model parameter for small basins in China. *Hydrological Processes*, *34*, 125–138.

Bennour, A., Jia, L., Menenti, M., Zheng, C., Zeng, Y., Barnieh, B. A., & Jiang, M. (2023). Assessing impacts of climate variability and land use/land cover change on the water balance components in the Sahel using Earth observations and hydrological modelling. *Journal of Hydrology: Regional Studies*, *47*, 101370.

Berghuijs, W. R., Gnann, S. J., & Woods, R. A. (2020). Unanswered questions on the Budyko framework. *Hydrological Processes*, *34*, 5699–5703.

Bichet, A., & Diedhiou, A. (2018). Less frequent and more intense rainfall along the coast of the Gulf of Guinea in West and Central Africa (1981 2014). *Climate Research*, *76*, 191–201.

Blatchford, M. L., Mannaerts, C. M., Njuki, S. M., Nouri, H., Zeng, Y., Pelgrum, H., Wonink, S., & Karimi, P. (2020). Evaluation of WaPOR V2 evapotranspiration products across Africa. *Hydrological Processes*, *34*, 3200–3221.

Bogning, S., Frappart, F., Paris, A., Blarel, F., Niño, F., Saux Picart, S., Lanet, P., Seyler, F., Mahé, G., Onguene, R., Bricquet, J. P., Etame, J., Paiz, M. C., & Braun, J. J. (2021). Hydro-climatology study of the Ogooué River basin using hydrological modeling and satellite altimetry. *Advances in Space Research*, *68*, 672–690.

Boogaard, H., Schubert, J., De Wit, A., Lazebnik, J., Hutjes, R., & Van der Grijn, G. (2020). Agrometeorological indicators from 1979 to present derived from reanalysis. Copernicus climate change service (C3S) climate data store (CDS).

Bruijnzeel, L. A. (2004). Hydrological functions of tropical forests: Not seeing the soil for the trees? *Agriculture, Ecosystems & Environment*, *104*, 185–228.

Brunner, M. I., Slater, L., Tallaksen, L. M., & Clark, M. (2021). Challenges in modeling and predicting floods and droughts: A review. *Wiley Interdisciplinary Reviews: Water*, *8*, e1520.

Budyko, M. I. (1974). *Climate and life*. No Title.

Camberlin, P., Barraud, G., Bigot, S., Dewitte, O., Makanzu Imwangana, F., Maki Mateso, J. C., Martiny, N., Monsieurs, E., Moron, V., Pellarin, T., Philippon, N., Sahani, M., & Samba, G. (2019). Evaluation of remotely sensed rainfall products over Central Africa. *Quarterly Journal of the Royal Meteorological Society*, *145*, 2115–2138.

Cao, Q., Liu, Y., Georgescu, M., & Wu, J. (2020). Impacts of landscape changes on local and regional climate: A systematic review. *Landscape Ecology*, *35*, 1269–1290. https://doi.org/10.1007/s10980-020-01015-7

Carrasco, L. R., Webb, E. L., Symes, W. S., Koh, L. P., & Sodhi, N. S. (2017). Global economic trade-offs between wild nature and tropical agriculture. *PLoS Biology*, *15*, e2001657.

Chawanda, C. J., Nkwasa, A., Thiery, W., & van Griensven, A. (2023). Combined impacts of climate and land-use change on future water resources in Africa. *Hydrology and Earth System Sciences Discussions*, *2023*, 1–32.

Chen, Z., Wang, W., Woods, R. A., & Shao, Q. (2021). Hydrological effects of change in vegetation components across global catchments. *Journal of Hydrology*, *595*, 125775.

Cheng, L., Zhang, L., Chiew, F. H., Canadell, J. G., Zhao, F., Wang, Y. P., Hu, X., & Lin, K. (2017). Quantifying the impacts of vegetation changes on catchment storage-discharge dynamics using paired-catchment data. *Water Resources Research*, *53*, 5963–5979.

Cheng, S., Cheng, L., Qin, S., Zhang, L., Liu, P., Liu, L., Xu, Z., & Wang, Q. (2022). Improved understanding of how catchment properties control hydrological partitioning through machine learning. *Water Resources Research*, *58*, e2021WR031412.

Cronin, D. T., Libalah, M. B., Bergl, R. A., & Hearn, G. W. (2014). Biodiversity and conservation of tropical montane ecosystems in the Gulf of Guinea, West Africa. *Arctic, Antarctic, and Alpine Research*, *46*, 891–904.

Derin, Y., Anagnostou, E., Berne, A., Borga, M., Boudevillain, B., Buytaert, W., Chang, C. H., Chen, H., Delrieu, G., Hsu, Y., Lavado-Casimiro, W., Manz, B., Moges, S., Nikolopoulos, E., Sahlu, D., Salerno, F., Rodríguez-Sánchez, J. P., Vergara, H., & Yilmaz, K. (2019). Evaluation of GPM-era global satellite precipitation products over multiple complex terrain regions. *Remote Sensing*, *11*, 2936.

Dezfuli, A. K., & Nicholson, S. E. (2013). The relationship of rainfall variability in western equatorial Africa to the tropical oceans and atmospheric circulation. Part II: The boreal autumn. *Journal of Climate*, *26*, 66–84.

Dike, V. N., Lin, Z.-H., & Ibe, C. C. (2020). Intensification of summer rainfall extremes over Nigeria during recent decades. *Atmosphere*, *11*, 1084.

DiMiceli, C., Townshend, J., Carroll, M., & Sohlberg, R. (2021). Evolution of the representation of global vegetation by vegetation continuous fields. *Remote Sensing of Environment*, *254*, 112271.

D'Odorico, P., Davis, K. F., Rosa, L., Carr, J. A., Chiarelli, D., Dell'Angelo, J., Gephart, J., MacDonald, G. K., Seekell, D. A., Suweis, S., & Rulli, M. C. (2018). The global food-energy-water nexus. *Reviews of Geophysics*, *56*, 456–531.

Donohue, R., Roderick, M., & McVicar, T. R. (2007). On the importance of including vegetation dynamics in Budyko's hydrological model. *Hydrology and Earth System Sciences*, *11*, 983–995.

Ebodé, V. B. (2022). Analysis of the Spatio-temporal rainfall variability in Cameroon over the period 1950 to 2019. *Atmosphere*, *13*, 1769.

Ebodé, V. B. (2023). Impact of climate and anthropogenic changes on current and future variability in flows in the Nyong River Basin (equatorial Central Africa). *Journal of Hydroinformatics*, *25*, 369–395.

Ebodé, V. B., Dzana, J. G., Nkiaka, E., Nnomo, B. N., Braun, J. J., & Riotte, J. (2022). Effects of climate and anthropogenic changes on current and future variability in flows in the So'o River Basin (south of Cameroon). *Hydrology Research*, *53*, 1203–1220.

Emerton, R., Zsoter, E., Arnal, L., Cloke, H. L., Muraro, D., Prudhomme, C., Stephens, E. M., Salamon, P., & Pappenberger, F. (2018). Developing a global operational seasonal hydro-meteorological forecasting system: GloFAS-seasonal v1. 0. *Geoscientific Model Development*, *11*, 3327–3346.

Ewane, E. B. (2021). Land use land cover change and the resilience of social-ecological systems in a sub-region in South west Cameroon. *Environmental Monitoring and Assessment*, *193*, 338. https://doi.org/10.1007/s10661-021-09077-z

Ferraz, S. F., Rodrigues, C. B., Garcia, L. G., Peña-Sierra, D., Fransozi, A., Ogasawara, M. E., Vasquez, K., Moreira, R. M., & Cassiano, C. C. (2021). How do management alternatives of fast-growing forests affect water quantity and quality in southeastern Brazil? Insights from a paired catchment experiment. *Hydrological Processes*, *35*, e14317.

Funk, C., Peterson, P., Landsfeld, M., Pedreros, D., Verdin, J., Shukla, S., Husak, G., Rowland, J., Harrison, L., Hoell, A., & Michaelsen, J. (2015). The climate hazards infrared precipitation with stations—A new environmental record for monitoring extremes. *Scientific Data*, *2*, 1–21.

Gan, G., Liu, Y., & Sun, G. (2021). Understanding interactions among climate, water, and vegetation with the Budyko framework. *Earth-Science Reviews*, *212*, 103451.

Gbohoui, Y. P., Paturel, J.-E., Tazen, F., Mounirou, L. A., Yonaba, R., Karambiri, H., & Yacouba, H. (2021). Impacts of climate and environmental changes on water resources: A multi-scale study based on Nakanbé nested watersheds in West African Sahel. *Journal of Hydrology: Regional Studies*, *35*, 100828.

Gebrechorkos, S. H., Hülsmann, S., & Bernhofer, C. (2020). Analysis of climate variability and droughts in East Africa using high-resolution climate data products. *Global and Planetary Change*, *186*, 103130.

Gebremicael, T., Mohamed, Y., & Van der Zaag, P. (2019). Attributing the hydrological impact of different land use types and their long-term dynamics through combining parsimonious hydrological modelling, alteration analysis and PLSR analysis. *Science of the Total Environment*, *660*, 1155–1167.

Gebremicael, T. G., Mohamed, Y. A., Zaag, P., Gebremedhin, A., Gebremeskel, G., Yazew, E., & Kifle, M. (2019). Evaluation of multiple satellite rainfall products over the rugged topography of the Tekeze-Atbara basin in Ethiopia. *International Journal of Remote Sensing*, *40*, 4326–4345.

Hasan, E., Tarhule, A., Kirstetter, P.-E., Clark, R., III, & Hong, Y. (2018). Runoff sensitivity to climate change in the Nile River Basin. *Journal of Hydrology*, *561*, 312–321.

Herrera, P. A., Marazuela, M. A., & Hofmann, T. (2022). Parameter estimation and uncertainty analysis in hydrological modeling. *Wiley Interdisciplinary Reviews: Water*, *9*, e1569.

Hirvonen, K., Machado, E. A., Simons, A. M., & Taraz, V. (2022). More than a safety net: Ethiopia's flagship public works program increases tree cover. *Global Environmental Change*, *75*, 102549.

Hua, W., Zhou, L., Chen, H., Nicholson, S. E., Raghavendra, A., & Jiang, Y. (2016). Possible causes of the Central Equatorial African long-term drought. *Environmental Research Letters*, *11*, 124002.

Huntington, J. L., Hegewisch, K. C., Daudert, B., Morton, C. G., Abatzoglou, J. T., McEvoy, D. J., & Erickson, T. (2017). Climate engine: Cloud computing and visualization of climate and remote sensing data for advanced natural resource monitoring and process understanding. *Bulletin of the American Meteorological Society*, *98*, 2397–2410.

Iroumé, A., Jones, J., & Bathurst, J. C. (2021). Forest operations, tree species composition and decline in rainfall explain runoff changes in the Nacimiento experimental catchments, South Central Chile. *Hydrological Processes*, *35*, e14257.

Jaramillo, F., Cory, N., Arheimer, B., Laudon, H., Van Der Velde, Y., Hasper, T. B., Teutschbein, C. & Uddling, J. (2018). Dominant effect of increasing forest biomass on evapotranspiration: Interpretations of movement in Budyko space. *Hydrology and Earth System Sciences*, *22*(1), 567–580.

Kingston, D., Massei, N., Dieppois, B., Hannah, D., Hartmann, A., Lavers, D., & Vidal, J.-P. (2020). Moving beyond the catchment scale: Value and opportunities in large-scale hydrology to understand our changing world. *Hydrological Processes*, *34*, 2292–2298.

Lehner, B., & Grill, G. (2013). Global river hydrography and network routing: Baseline data and new approaches to study the world's large river systems. *Hydrological Processes*, *27*, 2171–2186.

Lemenkova, P., & Debeir, O. (2023). Computing vegetation indices from the satellite images using GRASS GIS scripts for monitoring mangrove forests in the coastal landscapes of Niger Delta, Nigeria. *Journal of Marine Science and Engineering*, *11*, 871.

Li, D., Pan, M., Cong, Z., Zhang, L., & Wood, E. (2013). Vegetation control on water and energy balance within the Budyko framework. *Water Resources Research*, *49*, 969–976.

Li, Z., & Quiring, S. M. (2021). Identifying the dominant drivers of hydrological change in the contiguous United States. *Water Resources Research*, *57*, e2021WR029738.

Lu, W., Tang, J., Lu, C., Lu, C., Jia, Y., Sun, Q., He, X., & Zhang, X. (2022). Attribution analysis of the spatiotemporal variation in water balance in a typical semiarid basin in northern China. *Hydrological Processes*, *36*, e14651.

Luo, Y., Yang, Y., Yang, D., & Zhang, S. (2020). Quantifying the impact of vegetation changes on global terrestrial runoff using the Budyko framework. *Journal of Hydrology*, *590*, 125389.

Mahmoud, M. I., Campbell, M. J., Sloan, S., Alamgir, M., & Laurance, W. F. (2020). Land-cover change threatens tropical forests and biodiversity in the Littoral region, Cameroon. *Oryx*, *54*, 882–891.

Martens, B., Miralles, D. G., Lievens, H., van der Schalie, R., de Jeu, R. A. M., Fernández-Prieto, D., Beck, H. E., Dorigo, W. A., & Verhoest, N. E. (2017). GLEAM v3: Satellite-based land evaporation and root-zone soil moisture. *Geoscientific Model Development*, *10*, 1903–1925.

Mianabadi, A., Davary, K., Pourreza-Bilondi, M., & Coenders-Gerrits, A. (2020). Budyko framework; towards non-steady state conditions. *Journal of Hydrology*, *588*, 125089.

Moges, D. M., Virro, H., Kmoch, A., Cibin, R., Rohith, A., Martínez-Salvador, A., Conesa-García, C., & Uuemaa, E. (2023). How does the choice of DEMs affect catchment hydrological modeling? *Science of the Total Environment*, *892*, 164627.

Ndehedehe, C. E., Ferreira, V. G., & Agutu, N. O. (2019). Hydrological controls on surface vegetation dynamics over West and Central Africa. *Ecological Indicators*, *103*, 494–508.

Ndehedehe, C. E., Okwuashi, O., Ferreira, V. G., & Agutu, N. O. (2018). Exploring evapotranspiration dynamics over sub-Sahara Africa (2000–2014). *Environmental Monitoring and Assessment*, *190*, 1–19.

Neill, A. J., Birkel, C., Maneta, M. P., Tetzlaff, D., & Soulsby, C. (2021). Structural changes to forests during regeneration affect water flux partitioning, water ages and hydrological connectivity: Insights from tracer-aided ecohydrological modelling. *Hydrology and Earth System Sciences*, *25*, 4861–4886.

Ni, Y., Yu, Z., Lv, X., Qin, T., Yan, D., Zhang, Q., & Ma, L. (2022). Spatial difference analysis of the runoff evolution attribution in the Yellow River Basin. *Journal of Hydrology*, *612*, 128149.

Nkiaka, E. (2022). Water security assessment in ungauged regions using the water balance and water footprint concepts and satellite observations. *Hydrology Research*, *53*, 336–352.

Nkiaka, E., Bryant, R. G., Ntajal, J., & Biao, E. I. (2022). Evaluating the accuracy of gridded water resources reanalysis and evapotranspiration products for assessing water security in poorly gauged basins. *Hydrology and Earth System Sciences*, *26*, 5899–5916.

Nkiaka, E., Nawaz, N., & Lovett, J. (2016). Using self-organizing maps to infill missing data in hydro-meteorological time series from the Logone catchment, Lake Chad basin. *Environmental Monitoring and Assessment*, *188*, 1–12.

Nkiaka, E., Nawaz, N., & Lovett, J. (2018). Effect of single and multi-site calibration techniques on hydrological model performance, parameter estimation and predictive uncertainty: A case study in the Logone catchment, Lake Chad basin. *Stochastic Environmental Research and Risk Assessment*, *32*, 1665–1682.

Odongo, V. O., van Oel, P. R., van der Tol, C., & Su, Z. (2019). Impact of land use and land cover transitions and climate on evapotranspiration in the Lake Naivasha Basin, Kenya. *Science of the Total Environment*, *682*, 19–30.

Ota, T., Lonn, P., & Mizoue, N. (2020). A country scale analysis revealed effective forest policy affecting forest cover changes in Cambodia. *Land Use Policy*, *95*, 104597.

Richards, P. W., Walsh, R. P. D., Baillie, I. C., & Greig-Smith, P. (1996). *The tropical rain forest: An ecological study*. Cambridge University Press.

Riggs, R. M., Allen, G. H., Wang, J., Pavelsky, T. M., Gleason, C. J., David, C. H., & Durand, M. (2023). Extending global river gauge records using satellite observations. *Environmental Research Letters*, *18*, 064027.

Roffe, S. J., & van der Walt, A. J. (2023). Representation and evaluation of southern Africa's seasonal mean and extreme temperatures in the ERA5-based reanalysis products. *Atmospheric Research*, *284*, 106591.

Ryan, S. J., Palace, M. W., Hartter, J., Diem, J. E., Chapman, C. A., & Southworth, J. (2017). Population pressure and global markets drive a decade of forest cover change in Africa's Albertine rift. *Applied Geography*, *81*, 52–59.

Sagang, T. L.-B., Ploton, P., Viennois, G., Féret, J.-B., Sonké, B., Couteron, P., & Barbier, N. (2022). Monitoring vegetation dynamics with open earth observation tools: The case of fire-modulated savanna to forest transitions in Central Africa. *ISPRS Journal of Photogrammetry and Remote Sensing*, *188*, 142–156.

Sankarasubramanian, A., Vogel, R. M., & Limbrunner, J. F. (2001). Climate elasticity of streamflow in the United States. *Water Resources Research*, *37*, 1771–1781.

Shawul, A. A., Chakma, S., & Melesse, A. M. (2019). The response of water balance components to land cover change based on hydrologic modeling and partial least squares regression (PLSR) analysis in the Upper Awash Basin. *Journal of Hydrology: Regional Studies*, *26*, 100640.

Sidibe, M., Dieppois, B., Eden, J., Mahé, G., Paturel, J.-E., Amoussou, E., Anifowose, B., & Lawler, D. (2019). Interannual to multi-decadal streamflow variability in West and Central Africa: Interactions with catchment properties and large-scale climate variability. *Global and Planetary Change*, *177*, 141–156.

Skofronick-Jackson, G., Berg, W., Kidd, C., Kirschbaum, D. B., Petersen, W. A., Huffman, G. J., & Takayabu, Y. N. (2018). Global precipitation measurement (GPM): Unified precipitation estimation from space. In *Remote Sensing of Clouds and Precipitation* (pp. 175–193). Springer.

Vondou, D. A., Yepdo, Z. D., & Tchotchou, L. D. (2018). Diurnal cycle of convective cloud occurrences over Cameroon during June–August. *Journal of the Indian Society of Remote Sensing*, *46*, 829–845.

Wamucii, C. N., van Oel, P. R., Ligtenberg, A., Gathenya, J. M., & Teuling, A. J. (2021). Land use and climate change effects on water yield from East African forested water towers. *Hydrology and Earth System Sciences*, *25*, 5641–5665.

Wang, H., & Stephenson, S. R. (2018). Quantifying the impacts of climate change and land use/cover change on runoff in the lower Connecticut River Basin. *Hydrological Processes*, *32*, 1301–1312.

Wei, X., Liu, Y., Qi, L., Chen, J., Wang, G., Zhang, L., & Liu, R. (2023). Monitoring forest dynamics in Africa during 2000–2020 using a remotely sensed fractional tree cover dataset. *International Journal of Digital Earth*, *16*, 2212–2232.

Yang, D., Yang, Y., & Xia, J. (2021). Hydrological cycle and water resources in a changing world: A review. *Geography and Sustainability*, *2*, 115–122.

Yao, R., Cao, J., Wang, L., Zhang, W., & Wu, X. (2019). Urbanization effects on vegetation cover in major African cities during 2001–2017. *International Journal of Applied Earth Observation and Geoinformation*, *75*, 44–53.

Yonaba, R., Biaou, A. C., Koïta, M., Tazen, F., Mounirou, L. A., Zouré, C. O., Queloz, P., Karambiri, H., & Yacouba, H. (2021). A dynamic land use/-land cover input helps in picturing the Sahelian paradox: Assessing variability and attribution of changes in surface runoff in a Sahelian watershed. *Science of the Total Environment*, *757*, 143792.

Yue, K., de Frenne, P., Fornara, D. A., van Meerbeek, K., Li, W., Peng, X., Ni, X., Peng, Y., Wu, F., Yang, Y., & Peñuelas, J. (2021). Global patterns and drivers of rainfall partitioning by trees and shrubs. *Global Change Biology*, *27*, 3350–3357.

Zhang, L., Marshall, M., Vrieling, A., & Nelson, A. (2023). The divergence of energy-and water-balance evapotranspiration estimates in humid regions. *Journal of Hydrology*, *624*, 129971.

Zheng, H., Yang, Z. L., Lin, P., Wei, J., Wu, W. Y., Li, L., Zhao, L., & Wang, S. (2019). On the sensitivity of the precipitation partitioning into evapotranspiration and runoff in land surface parameterizations. *Water Resources Research*, *55*, 95–111.

SUPPORTING INFORMATION

Additional supporting information can be found online in the Supporting Information section at the end of this article.

How to cite this article: Nkiaka, E., & Okafor, G. C. (2024). Changes in climate, vegetation cover and vegetation composition affect runoff generation in the Gulf of Guinea Basin. *Hydrological Processes*, *38*(3), e15124. https://doi.org/10.1002/hyp.15124